ELSEVIER

Remote Sensing of Environment 77 (2001) 10–21

Remote Sensing of Environment

www.elsevier.com/locate/rse

AFRI — aerosol free vegetation index

Arnon Karnieli[a,*] Yoram J. Kaufman[b] Lorraine Remer[b] Andrew Wald[c]

[a]*The Remote Sensing Laboratory, Jacob Blaustein Institute for Desert Research, Ben Gurion University of the Negev, Sede Boker Campus 84990, Israel*
[b]*NASA/GSFC, Greenbelt, MD 20771, USA*
[c]*SAIC, Chantilly, VA 20151, USA*

Received 7 July 2000; received in revised form 20 December 2000; accepted 23 December 2000

Abstract

Aircraft measurements using a field spectrometer over variety of ground surfaces in Israel reveals that under clear sky conditions the shortwave infrared (SWIR) spectral bands around 1.6 and 2.1 μm are highly correlated with the visible — blue, green, and red — spectral bands. Empirical linear relationships, such as $\rho_{0.469} = 0.25\rho_{2.1}$; $\rho_{0.555} = 0.33\rho_{2.1}$; $\rho_{0.645} = 0.5\rho_{2.1}$; and $\rho_{0.645} = 0.66\rho_{1.6}$, were found to be statistically significant and consistent with previous findings. Based on the above relationships, a modified vegetation index (VI) is proposed and named Aerosol Free Vegetation Index (AFRI). Two versions of this VI are formulated as: $AFRI_{1.6} = (\rho_{NIR} - 0.66\rho_{1.6})/(\rho_{NIR} + 0.66\rho_{1.6})$ and $AFRI_{2.1} = (\rho_{NIR} - 0.5\rho_{2.1})/(\rho_{NIR} + 0.5\rho_{2.1})$. It is shown that under clear sky conditions, the AFRIs (and especially $AFRI_{2.1}$) closely resemble the Normalized Difference Vegetation Index (NDVI) and their values are almost identical. The advantage of the derived AFRIs, based on the ability of the SWIR bands is to penetrate the atmospheric column even when aerosols such as smoke or sulfates exist. Consequently, these indices have a major application in assessing vegetation in the presence of smoke, anthropogenic pollution, or volcanic plumes. This was demonstrated by applying the AFRI for a biomass burned forest in Brazil. Limited success of these indices is expected in case of dust due to presence of larger particles that are of similar size to the wavelength and therefore not transparent at 2.1 μm. The AFRIs can be implemented to data from any sensor that has the SWIR bands. Currently, the most commonly used of such instruments are the Landsat–Thematic Mapper (TM) and Advanced Thematic Mapper Plus (ETM+), Moderate Resolution Imaging Spectrometer (MODIS), Advanced Spaceborne Thermal Emission and Reflection (ASTER), and Japanese Earth Resources Satellite-Optical System (JERS-OPS). Although the $AFRI_{2.1}$ was demonstrated to perform better than the $AFRI_{1.6}$, the latter still can be used for the same application in conjunction with instruments that have onboard only the 1.6-μm band, such as Systeme Probatoire d'Observation del la Terre (SPOT4)–VEGETATION, Indian Remote Sensing (IRS-1C/D), and Resource-21.

1. Introduction

During the last three decades, and almost since the launch of the first remote sensing satellite, considerable efforts have been conducted to study the state and dynamics of vegetation by means of vegetation indices (VIs) (Bannari, Morin, Bonn, & Huete, 1995). Different VIs have been developed based on combinations of two or more spectral bands, assuming that multiband analysis would provide more information than a single one. Most VIs use radiance, surface reflectance (ρ), or apparent reflectance (measured at the top of the atmosphere) values in the red (R), and the near infrared (NIR) spectral bands and can be collected by any field, airborne, or spaceborne spectrometer or radiometer that covers these spectral regions. The indices have been proven to be well correlated with various vegetation parameters such as green biomass (Tucker, 1979), chlorophyll concentration (Buschmann & Nagel, 1993), leaf area index (Asrar, Fuchs, Kanemasu, & Hatfield, 1984), foliar loss and damage (Vogelmann, 1990), photosynthetic activity (Sellers, 1985), carbon fluxes (Tucker, Fung, Keeling, & Gammon, 1986), and more. Also, they have been found to be useful for different image analyses like crop classification (Ehrlich & Lambin, 1996), phenology (Justice, Townshend, Holbend, & Tucker, 1985), green coverage (Elvidge & Chen, 1995), and change detection (Lambin & Strahler, 1994).

The most widely used VI for agricultural, forestry, rangeland, and ecological applications is the Normalized Difference Vegetation Index (NDVI), formulated as (Rouse, Haas, Schell, Deering, & Harlan, 1974):

$$NDVI = (\rho_{NIR} - \rho_R)/(\rho_{NIR} + \rho_R). \quad (1)$$

* Corresponding author. Tel.: +972-8-659-6855; fax: +972-8-659-6704.
E-mail address: karnieli@bgumail.bgu.ac.il (A. Karnieli).

0034-4257/01/$ – see front matter
PII: S0034-4257(01)00190-0

This index, as well as its several other modifications that are less popular, is based on the difference between the maximum absorption of radiation in the red due to the chlorophyll pigments and the maximum reflection of radiation in the NIR due to the leaf cellular structure, and the fact that soil spectra, lacking these mechanisms, typically do not show such a dramatic spectral difference.

In spite of the intensive use of the NDVI and its variety of applications, several limitations of the index are known. Among these are the sensitivity for soil (especially dark and/or wet) background (Huete, 1987), saturation of the index values in case of dense and multilayered canopy (Lillesaeter, 1982), and sensitivity for atmospheric influence (Holben, 1986) since aerosol increases the apparent reflectance in the red band by scattering sunlight directly to the sensor and decreases to a lesser degree the reflectance in the NIR by absorption of sunlight (Fraser & Kaufman, 1985). Improvements of the NIR and red-based indices underwent in three directions:

1. Development of new VIs that minimize the background influence. The leading index in such an effort is the Soil-Adjusted Vegetation Index (SAVI) calculated as (Huete, 1988):

$$\mathrm{SAVI} = (\rho_{\mathrm{NIR}} - \rho_{\mathrm{R}})(1 + L)/(\rho_{\mathrm{NIR}} + \rho_{\mathrm{R}} + L) \quad (2)$$

where L is a canopy background adjustment factor that accounts for differential red and NIR extinction trough the canopy. Usually $L = 0.5$ is used for semivegetated areas. Other modifications are the Transformed SAVI (Baret, Guyot, & Major, 1989), Soil-Adjusted Ratio Vegetation Index (SAVI2) (Major, Baret, & Guyot, 1990), and Modified SAVI (Qi, Cheh, Huete, Kerr, & Sorooshian, 1994).

2. Kaufman and Tanré (1992) developed several VIs that directly correct the red radiance for aerosol effect by incorporating the blue (B) band. These are the atmospheric resistant vegetation index (ARVI; Eq. (3a)) and the soil-adjusted and atmospheric resistant vegetation index (SARVI; Eq. (4)):

$$\mathrm{ARVI} = (\rho_{\mathrm{NIR}} - \rho_{\mathrm{RB}})/(\rho_{\mathrm{NIR}} + \rho_{\mathrm{RB}}) \quad (3a)$$

in which the subscript RB denotes the red and blue bands, defined as (Eq. (3b)):

$$\rho_{\mathrm{RB}} = \rho_{\mathrm{R}} - \gamma(\rho_{\mathrm{B}} - \rho_{\mathrm{R}}) \quad (3b)$$

where γ is recommended by the authors to have a value of 1. Note that in ARVI, ρ stands for surface reflectance or apparent reflectance after correction for molecular scattering.

$$\mathrm{SARVI} = (\rho_{\mathrm{NIR}} - \rho_{\mathrm{RB}})(1 + L)/(\rho_{\mathrm{NIR}} + \rho_{\mathrm{RB}} + L) \quad (4)$$

where the value L is expected to be similar to that of Eq. (2). Another modification of this approach is the modified SARVI (Huete & Liu, 1994).

3. Development of the use of the shortwave infrared (SWIR) spectral bands for remote sensing of surface cover in the absence of aerosol effect (Kaufman & Remer, 1994; Kaufman et al., 1997) and construction of VIs that are independent of the aerosol loading (Kaufman & Remer, 1994; Miura, Huete, van Leewen, & Didan, 1988). The following section discusses this issue.

2. Use of the SWIR spectral bands for vegetation studies

In contrast to the wide use of the visible and NIR spectral bands, a limited use has been done with the SWIR spectral bands (1.6 and 2.1 μm) in vegetation studies. Tucker (1980) showed that the 1.6-μm band is the most sensitive to the liquid water content of leaves. Gao (1996) suggested to use the 1.24-μm band in a liquid water VI that maximizes sensitivity to liquid water content while, in contrast to NDVI, remaining insensitive to water vapor, minimizes the different sensitivity to the depth of penetration of solar radiation between the two bands used in the index. It was found that the 2.1-μm band is also very sensitive to liquid water content, but due to its lower reflectance, it is more similar to the 0.66-μm band in its dependence on surface cover than the 1.24- or 1.6-μm bands, and therefore has the potential to better mimic the NDVI without the aerosol interference (Kaufman et al., 1997).

Vogelman (1990) and Vogelmann and Rock (1988, 1989) show that VIs based on the ratio SWIR/NIR (1.6/0.83 and 2.1/0.83 μm) provide improved results in monitoring the state of deciduous and coniferous forests and in discriminating between different stages of the forest damage. Hunt and Rock (1989) tested the ability of such ratios to determine leaf relative water content and equivalent water thickness of different plant species with different leaf morphology. The 1.6-μm band also was shown to be sensitive to senescence vegetation (Qi, Marsett, & Heilman, 2000).

The use of the 2.1-μm band was suggested by Kaufman et al. (1997) for remote sensing of aerosol over land and for atmospheric correction of the Earth imagery. In this work, the authors underlined the characteristics of the 2.1-μm band:

- The 2.1-μm band is located in one of the atmospheric windows and, therefore, less influenced by atmospheric gasses such as O_2, O_3, H_2O, CO_2, etc.
- It is rather far from the Earth's peak emission at about 10 μm, and thus, in contrast to the 3.75-μm band (Holben, Vermote, Kaufman, Tanré, & Kalb, 1992), is not affected by uncertainties in the correction of emitted radiation.
- The wavelength of this band is much larger than the size of the most common types of aerosols, such as smoke or sulfates (but not larger than dust), and consequently penetrates the atmospheric column even if these aerosols exist (Kaufman & Tanré, 1994).
- Biophysiologically speaking, as chlorophyll absorption by healthy vegetation tends to reduce the reflectivity in the visible portion of the electromagnetic spectrum, liquid water in the plants, associated with the presence of chlorophyll, absorbs radiation in the 2.1-μm region.

• Similarly, factors that reduce reflectivity of soils in the visible region, such as soil moisture or self-shadow, act in the same direction in the SWIR region as well.

In framework of the efforts to develop applications of the 2.1-μm band for Terra — MOderate Resolution Imaging Spectrometer (MODIS) instrument, Kaufman et al. (1997) examined the relationships between the reflectivity of this band and those of the red and the blue ones using atmospheric corrected Landsat Thematic Mapper (TM) and Airborne Visible/InfraRed Imaging Spectrometer (AVIRIS) imagery. Their work reveals that high correlation exists between the surface reflectance in the blue (0.469 μm), red (0.645 μm), and 2.1 μm. Based on the large variety of ground features, it is shown that surface reflectance at 0.469 μm ($\rho_{0.469}$) and 0.645 μm ($\rho_{0.645}$) can be predicted from that at 2.1 μm ($\rho_{2.1}$), within $\Delta\rho = \pm 0.006$ for $\rho_{2.1} \leq 0.10$, using

$$\rho_{0.469} = 0.25\rho_{2.1} \tag{5a}$$

and

$$\rho_{0.645} = 0.5\rho_{2.1}. \tag{5b}$$

Miura, Huete, van Leeuwen, & Didan (1988) used the same assumptions as above (i.e., the SWIR spectral bands are relatively transparent to smoke, yet remain sensitive to green vegetation) to derive several SWIR-based VIs in order to test their ability to minimize atmospheric smoke contamination (Eqs. (6a) and (6b)):

$$\mathrm{NDVI_{MIR}} = (\rho_{\mathrm{NIR}} - \rho_{\mathrm{MIR}})/(\rho_{\mathrm{NIR}} + \rho_{\mathrm{MIR}}), \tag{6a}$$

$$\mathrm{SAVI_{MIR}} = (\rho_{\mathrm{NIR}} - \rho_{\mathrm{MIR}})(1 + L) / (\rho_{\mathrm{NIR}} + \rho_{\mathrm{MIR}} + L). \tag{6b}$$

In these VIs, MIR stands for either the 1.6- or 2.1-μm spectral bands that substitute for the red band in Eqs. (1) and (2). The authors recommended the use of the 2.1-μm band for vegetation monitoring over burned and smoked forest. However, they also admitted that these VIs do not function well when the area was not fully covered with green biomass.

The results presented above raised up the importance of studying the ability of the 1.6- and the 2.1-μm bands to predict the surface reflectance in the visible bands (0.469, 0.555, and 0.645 μm). Thus, the objective of this article is to explore relationships between the visible and the SWIR spectral bands and the possible use of the latter (1.6- and 2.1-μm bands) as a replacement of the red band in VI for conditions with high aerosol concentration, namely smoke. The relationships among the different bands were investigated in Israel, in a variety of ecosystems, and then the proposed method was implemented in Brazil for detecting vegetation under heavy-smoke condition.

3. Methods

3.1. Experimental design and data processing for the Israeli data set

A field campaign was conducted in Israel in May 1997. In the framework of this experiment, several instruments were installed on a light aircraft. These were an Analytic Spectral Devices (ASD) portable point spectrometer, a Sony video camera, and a Telatemp Model AG-42 infrared thermometer. These instruments were aligned to point down at nadir and synchronized for the same time to an accuracy of 1 s. In addition, a Magellan global positioning system was used for precise determination of the plane's location. The spectrometer has a spectral resolution of 3 nm between 0.4 and 1 μm, and about 10 nm resolution between 1 and 2.5 μm. The field of view had been set to 18°, corresponding to 100 m diameter of average area on the ground for a flight height of 300 m. This altitude is low enough to minimize the need for atmospheric correction of the spectral reflectance data, while averaging over sufficient large area (~ 100 m^2). Spectra were sampled once every 10 s. This article deals with a flight that was performed on May 6, 1997. It was a clear and dry day. Data were collected along a transect across the desert transition zone from the northern Negev desert to the coastal plain of the Mediterranean Sea. Average annual rainfall ranges from 100 mm in the south to 500 mm in the north. Note that the campaign was conducted in the peak biomass season for most natural vegetation and agricultural crops, although it was the period of harvesting the winter wheat and the beginning of summer crops, such as corn and cotton. Consequently, a variety of land cover types were targeted including agricultural fields of different crops, orchards, forests, grasslands, and bare surfaces. Naturally, these targets exhibit the whole range of vegetation cover, from exposed soils to fully covered green fields.

Target reflectance was determined by dividing ground radiance to that reflected from a barium sulfate ($BaSO_4$) plate. The plate radiance had to be measured on the ground before and after the flight because the overhead wing structure of the plane made in-flight plate measurements impossible. The target radiance measurements can therefore be separated from the white plate measurement by a considerable time and distance. Atmospheric correction based on the 6S radiative transfer code (Vermote, Tanre, Deuze, Herman, & Morcrette, 1997) was applied to account for the ~ 300 m air column difference between the plane and ground, while the white plate measurement does not. However, this effect is considered to be minimal due to the clear dry day and the short flight time (about 1.5 h around the local noon when the solar zenith angle changes slowly with time.

Forty-eight video images were selected from the in-flight videotape, representing different vegetation types and

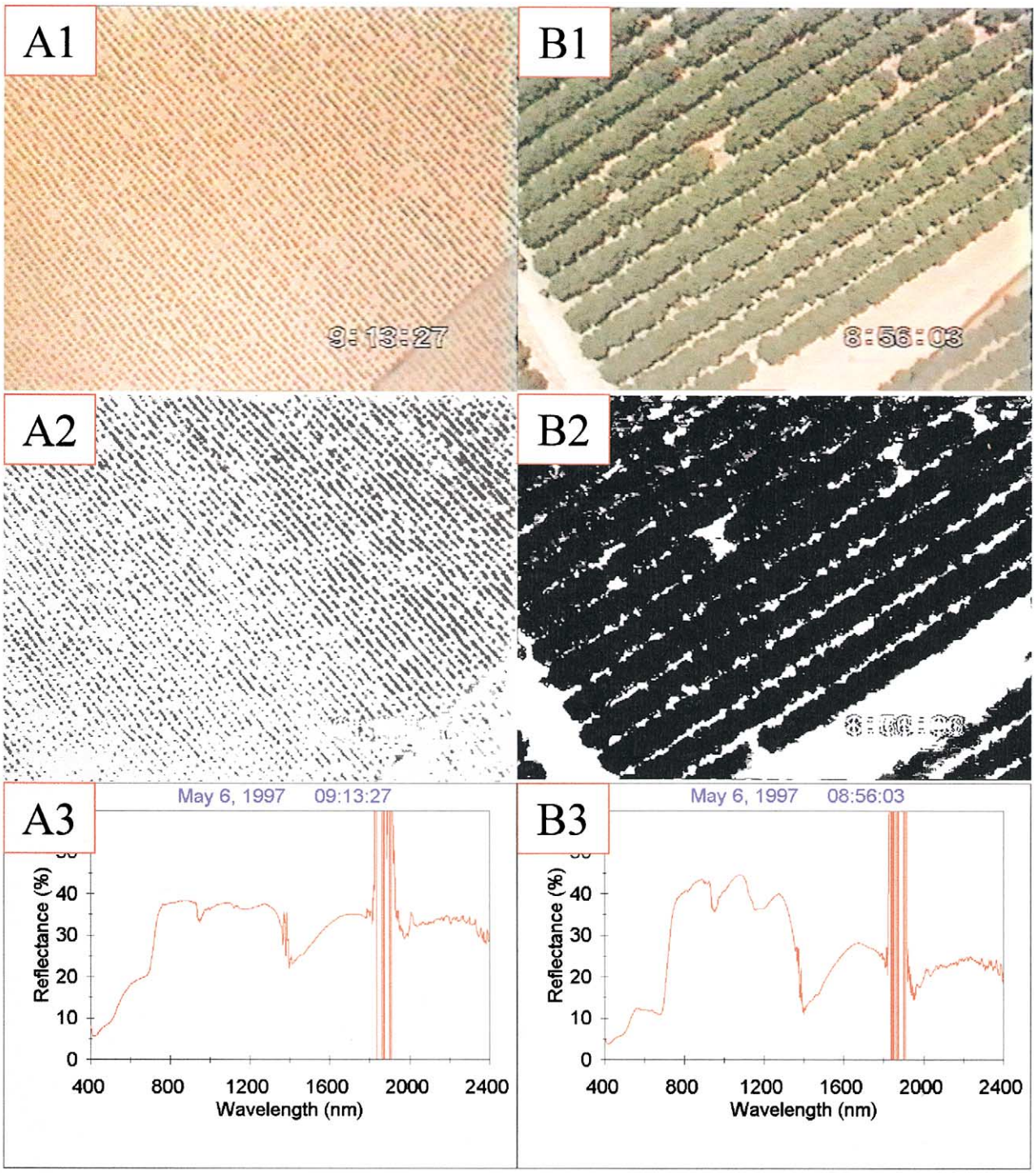

Fig. 1. Two examples of row video images (A1 and A2), classified images (B1 and B2), and their matched spectra (A3 and B3). Vegetation fractions are 19.2% and 75.8%, respectively).

percent cover. Fig. 1 (A1 and B1) represents two examples of such images. These video images were converted into digital form by means of a frame grabber. Using the supervised classification algorithm of the ERDAS-imagine software, the images were classified into two classes — vegetation and bare soil (Fig. 1, A2 and B2). Ratio between these classes reveals the vegetation fraction value (F) for each image (19.2% and 75.8% in the examples in Fig. 1). For the selected images, the time-matched spectra, acquired by the airborne-mounted ASD, were extracted

Table 1
Relevant MODIS spectral bands for examining relationships between different spectral bands in the visible, NIR, and SWIR regions

MODIS band	Wavelength (nm)				Spectral region
	Center	Minimum	Maximum	Width	
3	469	459	479	20	blue
4	555	545	565	20	green
1	645	620	670	50	red
2	860	841	876	25	NIR
6	1640	1628	1652	24	SWIR
7	2130	2105	2155	50	SWIR

(Fig. 1, A3 and B3). The ASD spectral bands were integrated according to several MODIS wavebands as described in Table 1.

3.2. Experimental design and data processing for the Brazilian data set

A field project called "Smoke, Clouds, and Radiation — Brazil (SCAR-B)" took place in the Amazon basin for studying characteristics of the above, related to fires during the biomass burning season (August–September) of 1995 (Kaufman et al., 1998). In the framework of this campaign, several NASA ER-2 aircraft flights were conducted. The ER-2 was equipped with a cross-track scanning spectrometer (MODIS airborne simulator), a downward looking lidar (cloud lidar system), a visible video camera system, and a hyperspectral imager (AVIRIS).

The AVIRIS is used to acquire reflected solar radiation in 224 narrow (10 nm width) contiguous spectral bands from 400 to 2500 nm (Vane et al., 1993). It is a whiskbroom imager, consisting of four spectrometers and linear array detectors. It flew at 20-km altitude, related to a 20-m spatial resolution at nadir and a 10-km swath width. Spectral and radiometric calibrations of the AVIRIS are performed yearly in the laboratory, while in-flight calibrations are conducted before, during, and after each flight season. The recently modified onboard calibrator is expected to achieve 1% stability in radiometric calibration.

The specific data set that was used for the current research was acquired over the Cuiabá region in the Amazon basin in Brazil on August 25, 1995. The image dimensions are 600×800 pixels (192 km^2).

4. Results and analysis

4.1. Relationships between the visible and the SWIR bands

Correlation matrix of the reflectance values corresponding with the 48 images that were selected from the Israeli flight images and related to the MODIS spectral bands are presented in Table 2. One might notice the relatively high correlation coefficient (r) values between each of the two SWIR bands and the three visible bands.

Scatterplots of the visible bands vs. the SWIR bands are presented in Fig. 2. Linear relationships between the 1.6-μm and the visible bands are calculated to be (Eqs. (7a)–(7c)):

$$\rho_{0.469} = -0.03 + 0.29\rho_{1.6}, \tag{7a}$$

$$\rho_{0.555} = -0.008 + 0.43\rho_{1.6}, \tag{7b}$$

$$\rho_{0.645} = -0.07 + 0.66\rho_{1.6}. \tag{7c}$$

These linear relationships can be improved by applying curvilinear relationships that produce slightly higher correlation coefficients than those presented in Table 2 (r=.96, .95, and .96 from the blue, green, and red bands, respectively). The curvilinear relationships can be formulated by second-order polynomial equations (Eqs. (8a)–(8c)):

$$\rho_{0.469} = 0.016 + 0.03\rho_{1.6} + 0.36\rho_{1.6}^2, \tag{8a}$$

$$\rho_{0.555} = 0.031 + 0.19\rho_{1.6} + 0.33\rho_{1.6}^2, \tag{8b}$$

$$\rho_{0.645} = 0.010 + 0.14\rho_{1.6} + 0.72\rho_{1.6}^2. \tag{8c}$$

Similarly, the linear relationships between the 2.1-μm band and the visible bands are formulated as (Eqs. (9a)–(9c)):

$$\rho_{0.469} = 0.008 + 0.23\rho_{2.1}, \tag{9a}$$

$$\rho_{0.555} = 0.05 + 0.31\rho_{2.1}, \tag{9b}$$

$$\rho_{0.645} = 0.004 + 0.52\rho_{2.1}. \tag{9c}$$

Since the intercepts are close to zero, these relationships can be generalized to those suggested by Kaufman et al. (1997), and we can assume that the reflectance values of the blue, green, and red bands are 0.25, 0.33, and 0.5 of the 2.1-μm band, respectively, where Eqs. (5a) and (5b) can be used as hypothetical models. Based on Kaufman et al. (1997) and other data sets, it is assumed that the hypothetical models are global values that can be used in different regions. The difference of the observed data in each of the visible bands from the respective hypothetical models can be

Table 2
Correlation matrix among reflectance values for 48 spectra of the Israeli data set

	$\rho_{0.469}$	$\rho_{0.555}$	$\rho_{0.645}$	$\rho_{0.86}$	$\rho_{1.6}$	$\rho_{2.1}$
$\rho_{0.469}$	1					
$\rho_{0.555}$	.92	1				
$\rho_{0.645}$	.98	.92	1			
$\rho_{0.86}$	.13	.43	.11	1		
$\rho_{1.6}$	**.94**	**.94**	**.95**	.31	1	
$\rho_{2.1}$	**.97**	**.90**	**.98**	.09	.95	1

Values in bold have special interest for the current study.

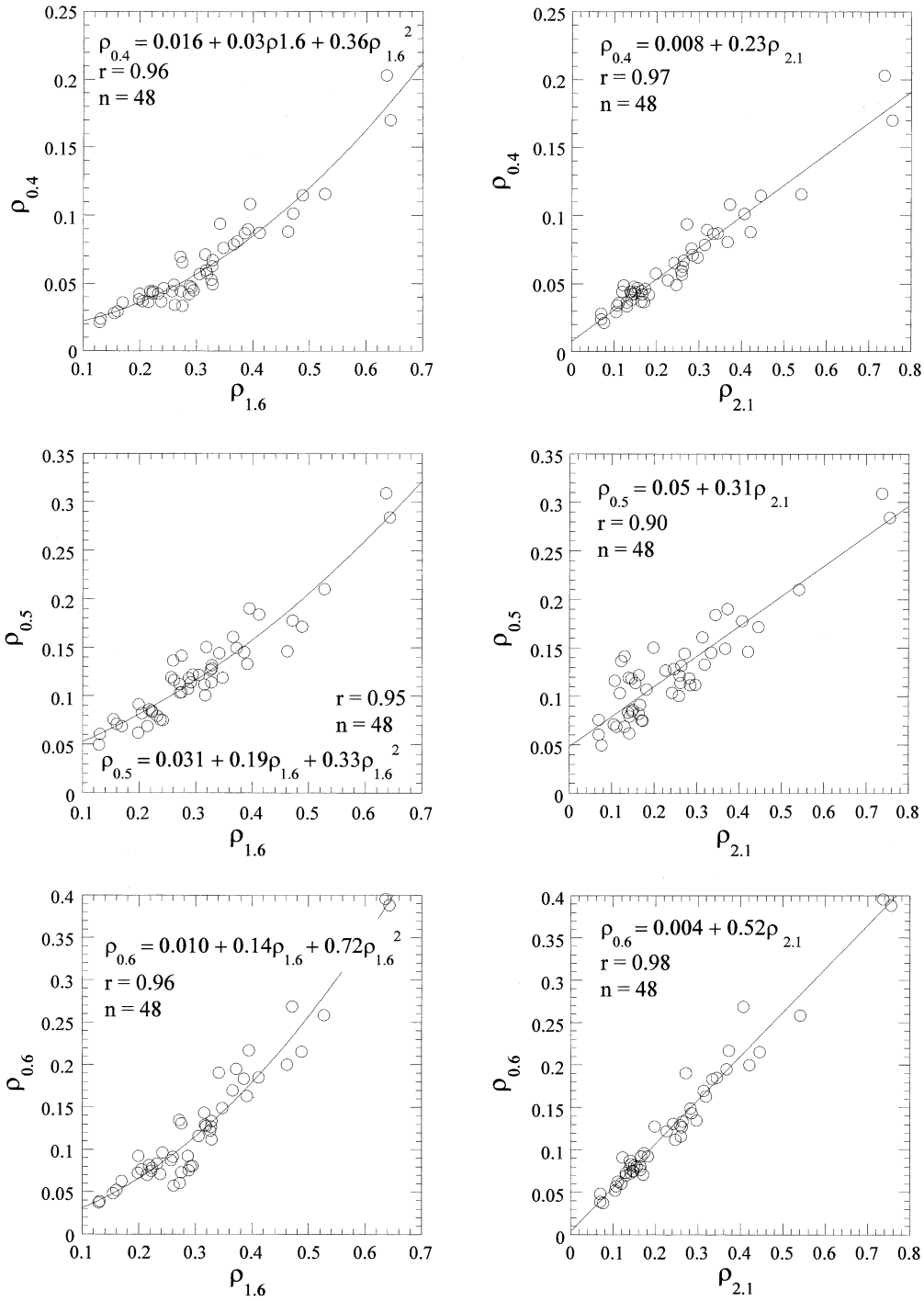

Fig. 2. Relationships between the visible spectral bands (blue, green, and red) and the SWIR bands (1.6 and 2.1 μm) for the Israeli data set.

obtained by the unbiased estimate of the variance (s^2, Eqs. (10a)–(10c)) (Walpole & Myers, 1985):

$$s^2_{0.469} = \sum(\rho_{0.469} - 0.25\rho_{2.1})^2/(n-2), \quad (10a)$$

$$s^2_{0.555} = \sum(\rho_{0.555} - 0.33\rho_{2.1})^2/(n-2), \quad (10b)$$

$$s^2_{0.645} = \sum(\rho_{0.645} - 0.50\rho_{2.1})^2/(n-2). \quad (10c)$$

where n is the number of observations ($n = 18$ in the current case). The resulted s^2 values were calculated to be 9.41E − 5, 2.46E − 3, and 3.06E − 4 for the blue, green, and red bands, respectively. These low values show how close the observed values are from the hypothetical model. For example, in the blue and red channels, which are used for remote sensing of

Table 3
Correlation matrix among various VIs for the Israeli data set

	NDVI	SAVI	ARVI	SARVI	$NDVI_{MIR1.6}$	$NDVI_{MIR2.1}$	$SAVI_{MIR1.6}$	$SAVI_{MIR2.1}$	$AFRI_{1.6}$	$AFRI_{2.1}$
NDVI	1									
SAVI	.91	1								
ARVI	**1.00**	.91	1							
SARVI	.93	1.00	.93	1						
$NDVI_{MIR1.6}$	**.96**	.93	**.96**	.93	1					
$NDVI_{MIR2.1}$	**.98**	.91	**.98**	.92	.98	1				
$SAVI_{MIR1.6}$	.94	.97	.94	.97	.99	.96	1			
$SAVI_{MIR2.1}$	.96	.97	.96	.97	.97	.98	.98	1		
$AFRI_{1.6}$	**.98**	.91	**.98**	.92	.97	1.00	.96	.98	1	
$AFRI_{2.1}$	**.98**	.90	**.98**	.91	.97	**1.00**	.95	.97	**1.00**	1

Values in bold have special interest for the current study.

aerosol, it corresponds to error in estimated surface reflectance of 0.01 and 0.017, respectively. This is within the acceptable error margins for aerosol studies (Kaufman et al., 1997).

Among the above relationships, the very high correlation coefficient between the red and the 2.1-μm band (r=.98) along with the corresponding low s^2 have a special interest since both bands can be corporately involved in a new VI, where the 2.1-μm band replaces the red one. Thus, it is hereby suggested to modify the NDVI (Eq. (1)) into a new index by the name of Aerosol FRee Vegetation Index (AFRI):

$$AFRI_{2.1} = (\rho_{NIR} - 0.5\rho_{2.1})/(\rho_{NIR} + 0.5\rho_{2.1}) \quad (11a)$$

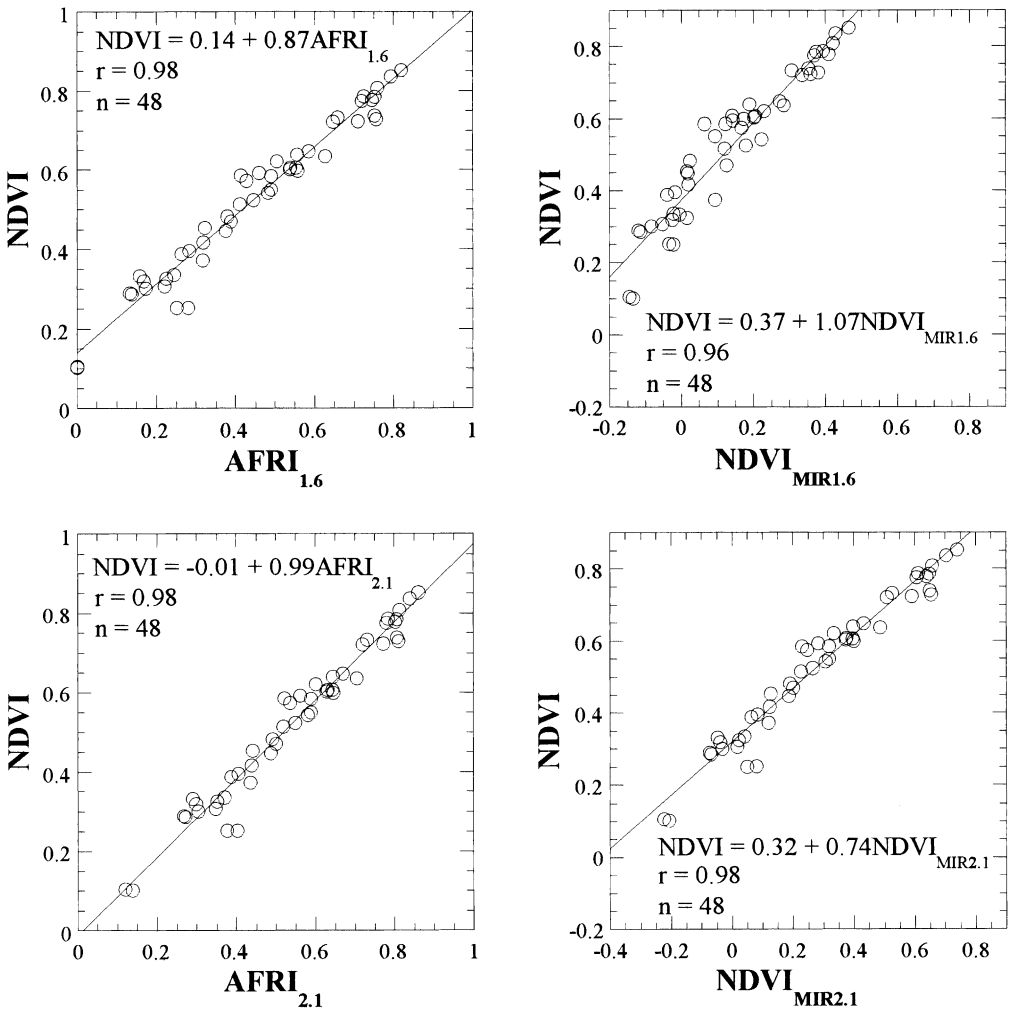

Fig. 3. NDVI vs. AFRI and NDVI vs. $NDVI_{MIR}$ for the Israeli data set.

or in case of the 1.6-μm band, based on Eq. (7c) (Eq. (11b)):

$$AFRI_{1.6} = (\rho_{NIR} - 0.66\rho_{1.6})/(\rho_{NIR} + 0.66\rho_{1.6}). \quad (11b)$$

Table 3 demonstrates a correlation matrix between all the above-mentioned VIs. General observation shows considerable high correlation ($r > .90$) among all VIs. However, several relationships have to be further discussed. On a clear day, as was occurred during the Israeli field campaign, the proposed $AFRI_{1.6}$ and $AFRI_{2.1}$ correlates highly ($r = .98$) with either NDVI or ARVI, which have a perfect correlation ($r = 1.0$) between them. Perfect correlation also exists between the $AFRI_{2.1}$ and the $NDVI_{MIR2.1}$. This is quite obvious since mathematically both indices relate linearly to each other. Also note that in this particular case, $AFRI_{1.6}$ and $AFRI_{2.1}$ correlate perfectly.

The relationships between the NDVI and the $AFRI_{1.6}$ and $AFRI_{2.1}$ are presented in Fig. 3. It can be seen that on a clear day the AFRI (especially $AFRI_{2.1}$) and the NDVI are related extremely close to each other with negligible intercept, and slope very close to the 1:1 line. Obviously, the $NDVI_{MIR}$ indices can function equally, but they cannot be conveniently used as illustrated in Fig. 3 due to their dynamic range. The $NDVI_{MIR}$ indices produce negative values and do not match the NDVI as close as the AFRIs do in terms of slope and intercept. It can be concluded that the $AFRI_{2.1}$ can be an excellent replacement for the NDVI and practically can be used for the applications listed above. In addition to these regular tasks, it is hypothesized that the proposed new VIs, $AFRI_{1.6}$ and $AFRI_{2.1}$, also have the advantage over the NDVI by their ability to penetrate the atmospheric column affected by smoke and thus offer additional function that cannot be implemented by the traditional NDVI. Such an application is presented in the next subsection.

For each of the selected images the vegetation fraction (F) was derived. Fig. 4 shows the surface reflectance at 0.469 and 0.645 μm as a function of the reflectance at 2.1 μm. The color of the symbol indicates the vegetation fraction, from green (high F) to brown (low F). It has to be remarked that the vegetation fraction is a weaker function of the reflectance at 2.1 μm than the reflectance in the visible channels. Apparently in this mix of vegetation covers, the reflectance is determined as much by the vegetation type as by the vegetation fraction. However, the dark pixels (reflectance at 2.1 μm < 0.15) were domi-

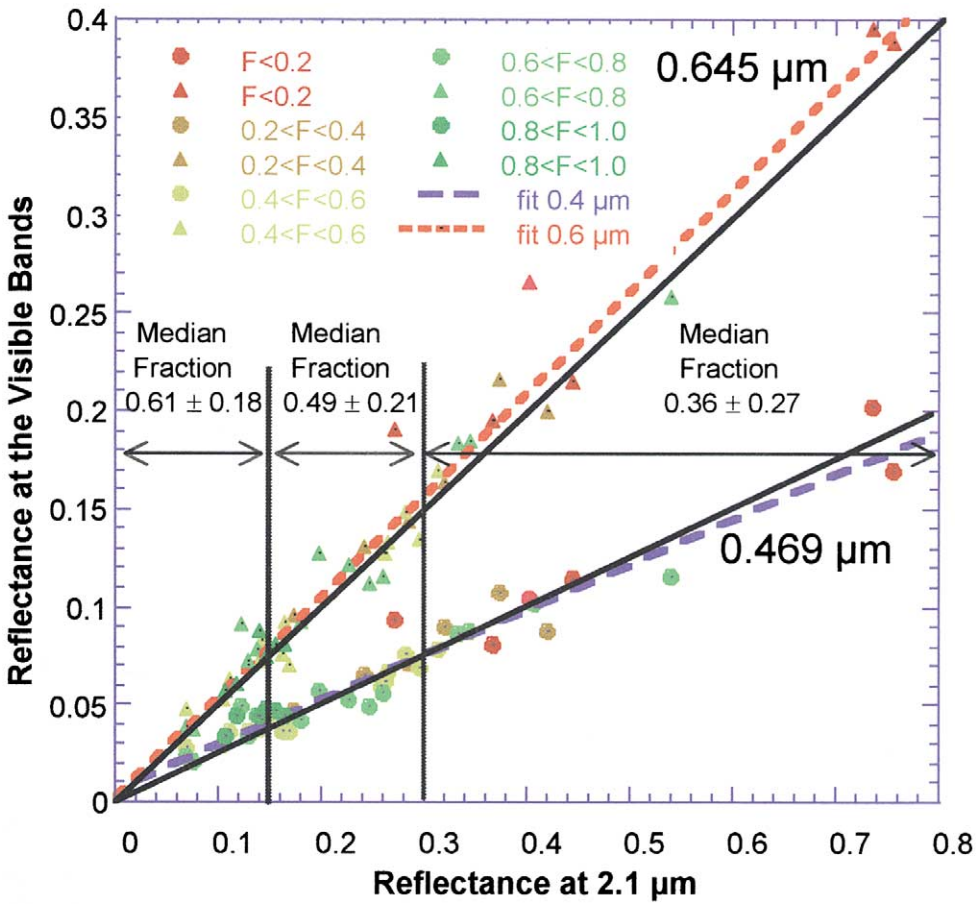

Fig. 4. The surface reflectance at 0.469 and 0.645 μm as a function of the reflectance at 2.1 μm. The color of the points changes from brown for vegetation fraction $F < 0.2$ to green for $F > 0.8$. The median value of the vegetation fraction for three ranges of the surface reflectance at 2.1 μm is given with the standard deviation. The red and blue lines are the best fits for all the data for each spectral channel. The black lines are the 25% and 50% lines for the blue and red, respectively, as hypothesized by Kaufman et al. (1997).

nated by high vegetation fractions of 0.61 ± 0.18, and the bright pixels by low vegetation fractions 0.36 ± 0.27. It is also interesting to note that the same linear relationship of close to 0.5 and 0.25 for the red and blue bands, respectively, that is observed for dark surfaces with high vegetation fraction continues for brighter surface with low vegetation fraction. Therefore, Fig. 4 demonstrates the transition from highly vegetated surfaces to sparsely vegetated with an increase in the reflectance at 2.1 μm and the visible bands. It also demonstrates that the linear relationships established for highly vegetated surfaces hold for sparse vegetation. In fact, the reflectance at 0.469 μm can be predicted from the reflectance at 2.1 μm, with an average absolute error of 0.007–0.010, independent of the range of the 2.1-μm band. The absolute error here is the average of $|0.25\rho_{2.1} - \rho_{0.469}|$. The average of the error in the red $|0.5\rho_{2.1} - \rho_{0.645}|$ increases with the 2.1-μm reflectance from 0.007 for the dark surfaces to 0.18 for the bright surfaces.

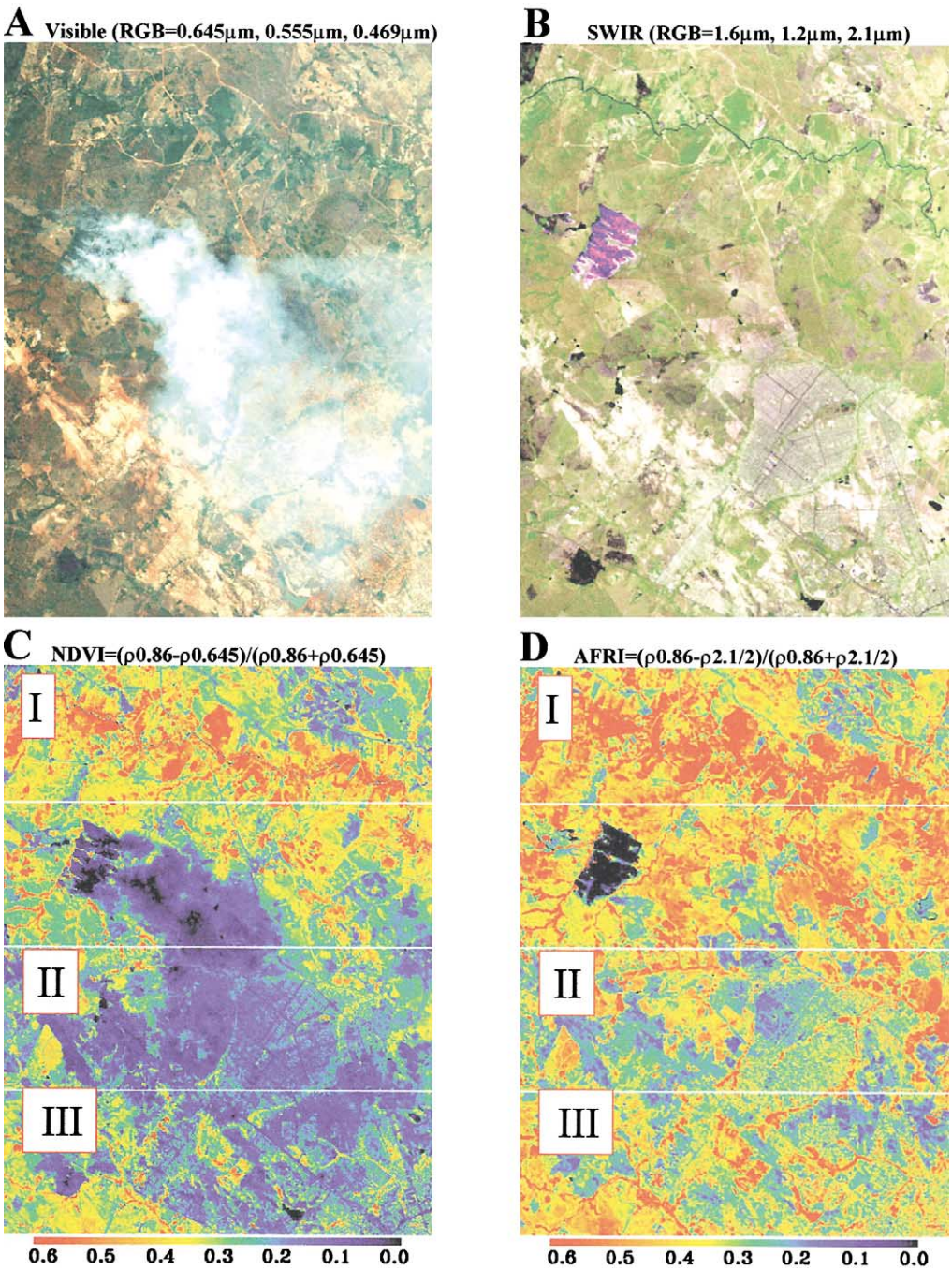

Fig. 5. AVIRIS image of one of the case studies for the SCAR-B campaign in Brazil, 1995. (A) True color composite (RGB = 0.645, 0.555, 0.469); (B) SWIR composite (RGB = 1.6, 1.2, 2.1); (C) NDVI; (D) AFRI: (I) smoke-free zone, (II) heavy-smoke zone, (III) light-smoke zone.

This linearity and predictability makes it possible to derive the aerosol optical thickness even over desert regions, as suggested earlier by Kaufman, Karnieli, and Tanré (2000).

4.2. Implementation of AFRI to Brazilian smoke

The area around Cuiabá, Brazil (9.9°S, 56.1°W) that was affected by heavy biomass burning on August 25, 1995, was used as one of the case studies for the SCAR-B field campaign (Kaufman et al., 1998). The fire and its smoke plume were scanned by the AVIRIS spectral imager on board of the ER-2 aircraft. Fig. 5A is a true color composite of the region, which covers 12×16 km^2, where RGB represent the red, green, and blue bands, respectively. Fig. 5B shows the same image by means of three SWIR bands. RGB is a composite of the 1.6-, 1.2-, and 2.1-μm bands, respectively. It demonstrates that the heavy smoke, which is visible in the shorter wavelengths, is almost transparent in the SWIR region and only the active fire source can be observed. Fig. 5C demonstrates the common NDVI product image. It can be noticed that the NDVI is highly contaminated by the smoke. The results are relatively low NDVI values that lead to a wrong interpretation of the state of vegetation masked by the smoke. On the other hand, the proposed VI, $AFRI_{2.1}$ (Eq. (11a)), which is based on the 2.1-μm band rather than the red (Fig. 5D), allows assessment of vegetation properties as well as other ground features beneath the smoke.

Fig. 5C and D were subdivided into four zones, 48 km^2 each. Zone I is characterized by smoke-free conditions, Zone II is characterized by heavy smoke, and Zone III is characterized by light smoke. The fourth zone, which contains the active fire source, was not used for the following analysis. The relationships between the NDVI and $AFRI_{2.1}$ were tested in Fig. 6 for the three zones in image in Fig. 5C and D. In the smoke-free zone, as expected, there is a high correlation between the two indices (r=.97). The scatterplot between them is close to the 1:1 line, with intercept of 0.01 and slope of 0.81 (Fig. 6A). Once smoke is introduced, the correlation coefficients drop to .79 and .69 for light and heavy no homogeneous smoke, respectively (Fig. 6B and C). Similarly, the slopes of the scatterplots drop to 0.78 and 0.59 for the light- and heavy-smoke regions.

Comparison between the derived NDVI and other VIs forthe Brazilian data set, in terms of correlation coefficients, is presented in Table 4. It can be seen that in the clear (smoke-free) area of the image (Fig. 5D: I), all VIs are highly correlated with the NDVI. However, under the smoky conditions (Fig. 5D: II and III), where the AFRIs show relatively low correlation coefficients, ARVI and SARVI, which are supposed to correct for the atmospher-icaerosols, remain highly correlative with the NDVI. Based on Fig. 5D, it is evident that all indices that are in correlation with NDVI cannot present the vegetation state as well as the AFRIs do.

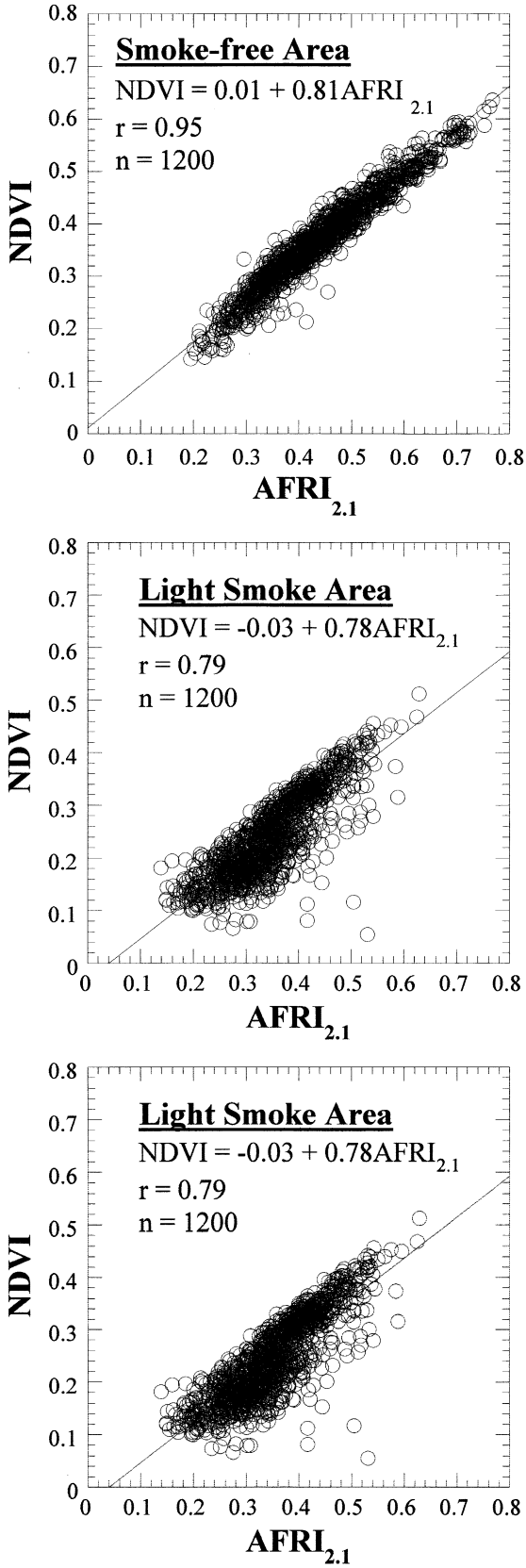

Fig. 6. Relationships between NDVI and $AFRI_{2.1}$ for the Brazilian data set under different atmospheric conditions: smoke-free zone, area with light zone, and zone with heavy smoke. Zones are corresponding to Fig. 5C and D.

Table 4
Correlation coefficients (r) between NDVI and other VIs under no smoke (clear), light-, and heavy-smoke conditions, calculated from the Brazilian data set

	NDVI		
	Clear	Light	Heavy
SAVI	.91	.88	.92
ARVI	.95	.86	.85
SARVI	.98	.90	.79
$AFRI_{1.6}$	.90	.38	.44
$AFRI_{2.1}$	.97	.79	.69

5. Concluding remarks

• For clear-sky conditions, the SWIR spectral bands around 1.6 and 2.1 μm are highly correlated with the visible — blue, green, and red — spectral bands. Simple linear relationships, such as $\rho_{0.469} = 0.25\rho_{2.1}$, $\rho_{0.555} = 0.33\rho_{2.1}$, $\rho_{0.645} = 0.5\rho_{2.1}$, and $\rho_{0.645} = 0.66\rho_{1.6}$, were found to be statistically significant.

• Based on the above relationships, two new VIs are proposed, denoted as $AFRI_{1.6}$ and $AFRI_{2.1}$. They are built similarly to the NDVI structure, but the respective portion of the SWIR bands substitute for the red band. In clear-sky conditions, the AFRIs (and especially $AFRI_{2.1}$) closely resemble the NDVI. Their values are almost identical.

• The advantage of the derived AFRIs is based on the ability of the SWIR bands to penetrate the atmospheric column even when aerosols such as smoke or sulfates exist. Consequently, these indices have a major application in assessing vegetation in the presence of smoke, anthropogenic pollution, or volcanic plumes. Limited success is expected in case of dust due to presence of larger particles that are of similar size to the wavelength, and therefore not transparent at 2.1 μm (see Kaufman et al., 2000).

• The 0.25 and 0.5 rules are independent of the vegetation fraction. The same linear relationships that are observed for dark surfaces with high vegetation cover continue for brighter surface with sparse vegetation cover.

• In terms of correlation with the NDVI, the AFRIs were found to be similar to the earlier proposed $NDVI_{MIR}$ indices. However, the latter indices produce negative values and are not as equivalent to the NDVI values as the AFRIs do. When correlating with the NDVI values, the intercept of the $NDVI_{MIR}$ is not 0 and its slope is not 1. Consequently, the AFRIs are more convenient to use and interpret.

• The AFRIs can be implemented with an image that is acquired by any sensor that contains the SWIR bands. Currently, the most commonly used of such instruments are the Landsat TM and ETM+, MODIS, and ASTER on board of the Terra satellite, and JERS-OPS.

• Although the $AFRI_{2.1}$ was demonstrated to perform better than the $AFRI_{1.6}$, the latter still can be used for the same application in conjunction with instruments that have onboard only the 1.6-μm band, such as SPOT4-VEGETATION, IRS-1C/D, and Resource-21.

References

Asrar, G., Fuchs, M., Kanemasu, E. T., & Hatfield, J. L. (1984). Estimating absorbed photosynthetic radiation and leaf area index from spectral reflectance of wheat. *Agronomy Journal*, *76*, 300–306.

Bannari, A., Morin, D., Bonn, F., & Huete, A. R. (1995). A review of vegetation indices. *Remote Sensing Review*, *13*, 95–120.

Baret, F., Guyot, G., & Major, D. J. (1989). TSAVI: a vegetation index which minimizes soil brightness effects on LAI and APAR estimation. *IGARRS'90, Proceedings of the 12th Canadian Symposium on Remote Sensing, Vancouver, BC, Canada, 10–14 July*, *3*, 1355–1358.

Buschmann, C., & Nagel, E. (1993). In vivo spectroscopy and internal optics of leaves as basis for remote-sensing of vegetation. *International Journal of Remote Sensing*, *14*, 711–722.

Ehrlich, D., & Lambin, E. F. (1996). Broad scale land-cover classification and interannual climatic variability. *International Journal of Remote Sensing*, *17*, 845–862.

Elvidge, C. D., & Chen, Z. K. (1995). Comparison of broad-band and narrow-band red and near-infrared vegetation indexes. *Remote Sensing of the Environment*, *54*, 38–48.

Fraser, R. S., & Kaufman, Y. J. (1985). The relative importance of scattering and absorption in remote sensing. *IEEE Transactions on Geoscience and Remote Sensing*, *23*, 625–633.

Gao, B.-C. (1996). NDWI — a normalized difference water index for remote sensing of vegetation liquid water from space. *Remote Sensing of the Environment*, *58*, 257–266.

Holben, B. (1986). Characteristics of maximum-value composite images from temporal AVHHR data. *International Journal of Remote Sensing*, *7, 1417–1434.*

Holben, B., Vermote, E., Kaufman, Y., Tanré, D., & Kalb, V. (1992). Aerosol retrieval over land from AVHRR data — application for atmospheric correction. *IEEE Transactions on Geoscience and Remote Sensing*, *30*, 212–232.

Huete, A. (1987). Soil influence in remote sensed vegetation-canopy spectra. In: C. Elachi (Ed.), *Introduction to the physics and techniques of remote sensing* (pp. 107–141). New York: Wiley-Interscience.

Huete, A. (1988). A soil-adjusted vegetation index (SAVI). *Remote Sensing of the Environment*, *25*, 295–309.

Huete, A., & Liu, H. Q. (1994). An error and sensitivity analysis of the atmospheric- and soil-correcting variants of the NDVI for the MODIS-EOS. *IEEE Transactions on Geoscience and Remote Sensing*, *32*, 897–905.

Hunt, E. R., & Rock, B. N. (1989). Detection of changes in leaf water content using near- and middle-infrared reflectances. *Remote Sensing of the Environment*, *30*, 43–54.

Justice, C. O., Townshend, J. R. G., Holben, B. N., & Tucker, C. J. (1985). Analysis of the phenology of global vegetation using meteorological satellite data. *International Journal of Remote Sensing*, *6*, 1271–1318.

Kaufman, Y. J., Hobbs, P. V., Kirchhoff, V. W. J. H., Artaxo, P., Remer, L. A., Holben, B. N., King, M. D., Ward, D. E., Prins, E. M., Longo, K. M., Mattos, L. F., Nobre, C. A., Spinhirne, J. D., Ji, Q., Thompson, A. M., Gleason, J. F., Christopher, S. A., & Tsay, S. C. (1998). Smoke, Clouds, Radiation — Brazil (SCAR-B) experiment. *Journal of Geophysical Research*, *103*, 31783–31808.

Kaufman, Y. J., Karnieli, A., & Tanré, D. (2000). Detection of dust over deserts using satellite data in the solar wavelengths. *IEEE Transactions on Geoscience and Remote Sensing*, *38*, 525–531.

Kaufman, Y. J., & Remer, L. A. (1994). Detection of forests using mid-IR reflectance — an application for aerosol studies. *IEEE Transactions on Geoscience and Remote Sensing*, *32*, 672–683.

Kaufman, Y. J., & Tanré, D. (1992). Atmospherically resistant vegetation index (ARVI) for EOS-MODIS. *IEEE Transactions on Geoscience and Remote Sensing*, *30*, 261–270.

Kaufman, Y. J., & Tanré, D. (1994). Effect of variations in supersaturation on the formation of cloud condensation nuclei. *Nature*, *369*, 45–48.

Kaufman, Y. J., Wald, A. E., Remer, L. A., Gao, B.-C., Li, R.-R., & Luke, F. (1997). The MODIS 2.1-μm band correlation with visible reflectance for use in remote sensing of aerosol. *IEEE Transactions on Geoscience and Remote Sensing*, *35*, 1286–1298.

Lambin, E. F., & Strahler, A. H. (1994). Change-vector analysis in multitemporal space: a tool to detect and categorize land-cover change processes using high temporal-resolution satellite data. *Remote Sensing of the Environment*, *48*, 231–244.

Lillesaeter, O. (1982). Spectral reflectance of partly transmitting leaves: laboratory measurements and mathematical modeling. *Remote Sensing of the Environment*, *12*, 247–254.

Major, D. J., Baret, F., & Guyot, G. (1990). A ratio vegetation index adjusted for soil brightness. *Remote Sensing of the Environment*, *11*, 727–740.

Miura, T., Huete, A. R., van Leeuwen, W. J. D., & Didan, K. (1988). Vegetation detection trough smoke-filled AVIRIS images: an assessment using MODIS band passes. *Journal of Geophysical Research*, *103*, 32001–32011.

Qi, J., Chehbouni, A., Huete, A., Kerr, Y. H., & Sorooshian, S. (1994). A modified soil adjusted vegetation index. *Remote Sensing of the Environment*, *48*, 119–126.

Qi, J., Marsett, R. C., & Heilman, P. (2000). Rangeland vegetation cover estimation from remotely sensed data. *Proceedings of the 2nd International Conference on Geospatial Information in Agriculture and Forestry, Volume II, Lake Buena Vista, Florida, 10–12 January*, II234–II252.

Rouse, J. W., Haas, R. H., Schell, J. A., Deering, D. W., & Harlan, J. C. (1974). *Monitoring the vernal advancements and retrogradation (greenwave effect) of nature vegetation* (371 pp). NASA/GSFC Final Report. Greenbelt, MD: NASA.

Sellers, P. J. (1985). Canopy reflectance, photosynthesis and transpiration. *International Journal of Remote Sensing*, *6*, 1335–1372.

Tucker, C. J., Fung, I. Y., Keeling, C. D., & Gammon, R. H. (1986). Relationship between atmospheric CO_2 variations and a satellite-derived vegetation index. *Nature*, *319*, 195–199.

Tucker, J. C. (1979). Red and photographic infrared linear combination for monitoring vegetation. *Remote Sensing of the Environment*, *8*, 127–150.

Tucker, J. C. (1980). A critical review of remote sensing and other methods for non-destructive estimation of standing crop biomass. *Grass and Forage Science*, *35*, 177–182.

Vane, G., Green, R. O., Chrien, T. G., Enmark, H. T., Hansen, E. G., & Porter, W. M. (1993). The airborne visible infrared imaging spectrometer (AVIRIS). *Remote Sensing of the Environment*, *44*, 127–143.

Vermote, E. F., Tanré, D., Deuze, J. L., Herman, M., & Morcrette, J. J. (1997). Second simulation of the satellite signal in the solar spectrum: an overview. *IEEE Transactions on Geoscience and Remote Sensing*, *35*, 675–686.

Vogelmann, J. E. (1990). Comparison between two vegetation indices for measuring different types of forest damage in north-eastern United States. *International Journal of Remote Sensing*, *11*, 2281–2297.

Vogelmann, J. E., & Rock, B. N. (1988). Assessing forest damage in high-elevation coniferous forests in Vermont and New Hampshire using Thematic Mapper data. *Remote Sensing of the Environment*, *24*, 227–246.

Vogelmann, J. E., & Rock, B. N. (1989). Use of Thematic Mapper data for the detection of forest damage caused by the pear thrips. *Remote Sensing of the Environment*, *30*, 217–225.

Walpole, R. E., & Myers, R. H. (1985). *Probability and statistics for engineers and scientists*. New York: MacMillan (639 pp.).